ELSEVIER

Surface Science 423 (1999) 208–224

surface science

Growth kinetics of decanethiol monolayers self-assembled on Au(111) by molecular beam deposition: An atomic beam diffraction study

P. Schwartz [a,b,1], F. Schreiber [a,2], P. Eisenberger [a,c,3], G. Scoles [a,d,*]

[a] *Princeton Materials Institute, Princeton University, Princeton, NJ 08544, USA*
[b] *Department of Astrophysical Sciences, Princeton University, Princeton, NJ 08544, USA*
[c] *Physics Department, Princeton University, Princeton, NJ 08544, USA*
[d] *Chemistry Department, Princeton University, Princeton, NJ 08544, USA*

Received 30 January 1998; accepted for publication 30 November 1998

Abstract

A low-energy atom diffraction study of the self-assembly of decanethiol on Au(111) is presented that includes both the growth kinetics and the adsorption energetics for this model system of soft/hard interfaces. Initial dosing on bare gold very rapidly forms the known low-density, lying-down, striped monolayer with a sticking coefficient close to unity. Further dosing results in an intermediate state that lacks long-range order. After an initial 'induction time', the final, dense, standing-up $c(4\times2)$ phase grows from this intermediate state with a growth rate that is about 500 times slower than that of the striped phase. Our data are consistent with the X-ray results of Eberhardt et al. (A. Eberhardt, P. Fenter, P. Eisenberger, Surf. Sci., 397 (1998) L285) where the growth rate of the $c(4\times2)$ phase was studied and found to depend linearly on the pressure at low pressures and high temperatures, changing to a quadratic dependence at higher pressures and lower temperatures. At still higher pressures and lower crystal temperatures, we find that the growth rate pressure dependence weakens substantially, becoming less than linear. In order to understand this behavior, an investigation of the adsorption energetics of thiols on top of the monolayer surface at different points during the growth is made. These results show that in the low-T, high-P regime, the $c(4\times2)$ phase grows under a full cover of molecules physisorbed on top of the (decaying) striped phase. This explains the weakening in the pressure dependence mentioned above since, at the limit of growth under a thick overlayer, the growth rate is expected to become pressure-independent.

Keywords: Adsorption kinetics; Alkanethiol; Atom–solid reactions and diffraction-elastic; Chemical vapor deposition; Chemisorption; Gold; Self-assembly; Thermal desorption

* Corresponding author. Present address: Chemistry Department, Princeton University, Princeton, NJ 08544, USA. Fax: +1 609-258-6665 e-mail: gscoles@princeton.edu.
[1] Present address: The Colorado College Physics Department, Colorado Springs, CO 80903, USA.
[2] Present address: MPI für Metallforschung, Heisenbergstr. 1, 70569 Stuttgart, Germany.
[3] Present address: Colombia Earth Institute and Lamont Earth Observatory, Colombia University, New York, NY 10027, USA.

0039-6028/99/$ – see front matter
PII: S0039-6028(98)00907-8

1. Introduction

Self-assembled monolayers (SAMs) are presently intensely studied as model systems for basic research that should lead to a better understanding of the physics of soft matter in two dimensions (including complex biological systems such as membranes) and the nature of organic/inorganic interfaces [1–3]. They also receive considerable attention because of potential technological applications such as corrosion resistance and the nanofabrication of electronic components. Whether the goal of the research is basic or applied science, a firm understanding of the equilibrium SAM structure, along with an understanding of the structure and stability of the intermediate phases that may be formed in the self-assembly process, is an essential requirement.

The equilibrium low- and high-coverage structures of alkanethiol SAMs on Au(111) is now well established, although a certain amount of refinement is still required. At low coverage, Θ, a phase is formed that is comprised of molecules lying down on the surface in a rectangular $p \times \sqrt{3}$ unit cell, the length of which (p, in units of the Au spacing of 2.88 Å) is chain-length-dependent and very close to twice that found in the corresponding bulk phases of the molecule [4,5]. In this phase, the molecules are believed to lie sulfur to sulfur, with the hydrocarbon chains stretching out in opposite directions. For decanethiol [$CH_3(CH_2)_9SH$, referred to as 'C10' throughout this paper], p is approximately 11, corresponding to a spacing of about 32 Å. This phase is referred to as the striped phase, as the rows of ordered thiol chains appear as pinstripes in STM images [6]. At high coverage, the thiols adopt a standing up phase with an average chain–chain distance of 5 (equal to $\sqrt{3} \times 2.88$)Å. However, not all the molecules in the unit cell are identical, resulting in what is commonly referred to as $c(4 \times 2)$ superstructure of a hexagonal $(\sqrt{3} \times \sqrt{3})R30^\circ$ lattice ['$c(4 \times 2)$' in short notation] [7,8]. Other saturation coverage hexagonal superlattices have also been reported, as well as a simple hexagonal phase [2,9–12]. Other intermediate phases such as the $(5\sqrt{3} \times \sqrt{3})R30^\circ$ phase have also been reported, which are very likely to occur at coverages that are higher than that of the stripes, but lower than that needed to produce the $c(4 \times 2)$ [11–14]. These lower-coverage phases have been prepared both directly by gas phase deposition, and by thermal desorption of thiols from the densest phase [4].

In contrast to their structure, the *growth kinetics* of SAMs has not been investigated as thoroughly since it depends in a complex way on the crystal temperature, the impingement rate and the coverage. Until now, only a small area of this rich parameter space has been investigated. The recent finding [15] that the growth rate, R, of the $c(4 \times 2)$ phase increases linearly with the thiol impingement rate, P, in a regime of low P and high crystal temperatures, T, but increases quadratically in a regime of high P and low T, is a further manifestation that the growth process in these systems is far from trivial and requires careful investigation.

In a handful of previous studies, growth has been studied from solution [16–21]. Liu et al. identify a lying down phase in the early stages of growth [19], whereas Georgiadis et al. identify, by means of SPRS (surface plasmon resonance spectroscopy), three distinct growth phases with different rates and solvent dependencies [20]. Here, as in a parallel study using grazing incidence X-ray diffraction (GIXD) [21], we have chosen growth from the vapor as it allows us to follow the molecular-level processes in situ using a structure-sensitive technique. Among the few studies employing vapor phase deposition is a recent STM investigation [22] where detailed images of various growth stages were provided. Although a complete analysis of the kinetics was not performed, on a qualitative level, the evolution and appearance of the different structures seem to agree with the data presented below. However, it is useful to note that STM is sensitive to *local* conditions and, therefore, is also able to resolve poorly ordered structures, whereas helium and X-ray diffraction detect the *average* behavior of the whole system, making the two classes of methods complementary.

The present study focuses on low-energy atom diffraction (LEAD), which is a non-perturbative and non-destructive method with unique surface specificity. The scattering of the non-penetrating helium beam yields direct information on the struc-

ture of the uppermost surface at all stages of the growth. In contrast, using GIXD, it is more difficult to follow the initial stages of the growth (i.e. the formation of the striped phase and its decay), but one can obtain at all times information on the monolayer–substrate interface. Although this paper is intended as a self-standing report of the results obtained from LEAD, it has to be seen in connection with parallel work done in our group where related issues were investigated using complementary techniques, such as GIXD [21] and temperature-programmed desorption (TPD) [23]. A brief summary of all three investigations also appears in the literature [24].

This paper is organized as follows. In Section 2, we first introduce the LEAD apparatus and explain the changes that were implemented for the present studies. We then describe the experimental procedures employed for the investigation of the growth. In Section 3, we present the experimental results. In particular, we discuss the following:

- The uptake curve of the molecules and the monolayer structural evolution. The thiol uptake is found to occur in two (or possibly three) steps, each with its own characteristic growth rate.
- The dependence of the growth rates on pressure and temperature.
- The measurement of the adsorption energetics of the molecules on the SAM surface at different stages of growth.

A summary and conclusions follow in Section 4.

2. Experimental

2.1. The scattering apparatus

The general layout of the helium beam surface diffraction apparatus has been described in previous publications [5,14]. Briefly, it consists of two differentially pumped vacuum chambers. In the first, a helium beam is produced by supersonic expansion from a cold source into a background pressure of approximately 10^{-4} Torr. The source is usually at 70 K, but its temperature can be controlled to change the energy of the He beam, and thus the incident wave vector. The beam passes via a skimmer into the second chamber (Fig. 1) with a base pressure of 10^{-7} Torr where it strikes the crystal mounted on a manipulator. The diffracted beam is detected by a rotating bolometer that is thermally anchored to a 1.6 K pumped helium cryostat. The detector/crystal assembly is located inside two concentric radiation shields cooled with liquid nitrogen, which keep thermal radiation from warming the bolometer (and its cryostat), and define an inner space that is very effectively cryopumped, keeping estimated pressures of impurities as low as 10^{-12} Torr near the crystal when the helium cryostat is at 1.6 K. In order to perform the present study, a series of

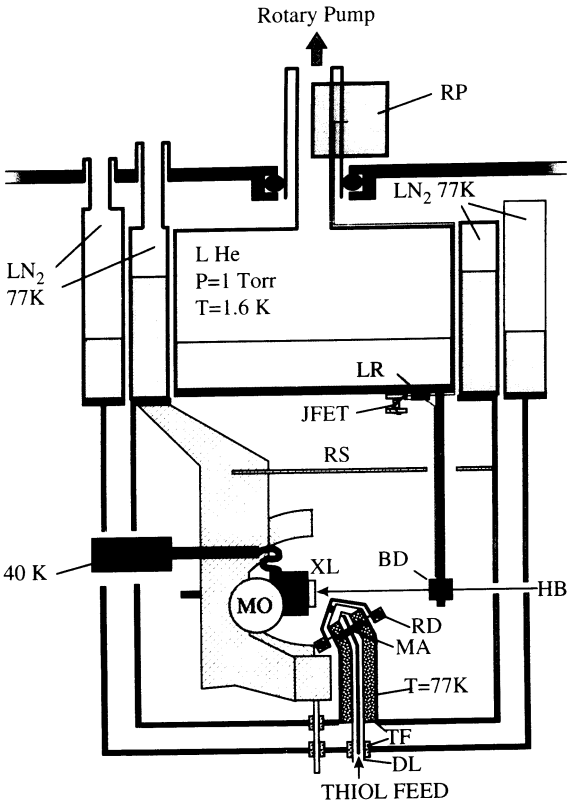

Fig. 1. Sketch of the inner part of the helium scattering apparatus with the newly implemented doser (RS: radiation shield; XL: crystal; BD: bolometer detector; MO: motor; RD: rotatable doser shutter; MA: actuator magnet; TF: Teflon spacer/insulator; DL: dose line, HB: incident helium beam; LR: load resistor; RP: rotatable preamplifier.). The inner part of the chamber is cryogenically shielded from the outer part and therefore also very effectively cryopumped.

improvements were implemented, as described below (see also Fig. 1) [25]:

1. A heated dosing system was constructed with a 0.60 mm nozzle located 11 mm from the center of the crystal surface. Insulating Teflon spacers support the heated copper dosing line inside a larger 77 K copper pipe, which shields the inner chamber from the warm dosing line. A rotatable shutter is also kept at 77 K and is actuated by means of a magnetic coil acting on small magnets rotating with the shutter. The dosing line is fed from the outside by means of a bakeable UHV stainless-steel manifold. The thiol flux to the crystal surface is varied by regulating the temperature of the liquid thiol in an outside reservoir controlling the pressure in the line.
2. Radiation shields (RS) were installed to protect the 1.6 K liquid helium cryostat from thermal radiation from the crystal, and collimating apertures were made for the bolometer. This allows the bolometer to remain cold enough to take data at crystal temperatures well above room temperature. The detection efficiency only drops to 50% when the crystal is heated to 400 K, whereas previously, useful data could not be collected at crystal temperatures above 200 K. The increased radiation shielding also allows for smaller liquid helium consumption during experiments requiring longer times at higher crystal temperatures.
3. The He source nozzle, originally attached to the cold head of a closed cycle refrigerator, was mounted on the wall separating the source chamber and the scattering chamber by means of a stepper motor controlled x–y–z translation stage. This lowered vibration-induced fluctuations of the main beam from as much as 20% to less than 0.2%. The nozzle was then thermally connected to the refrigerator by means of a copper braid.
4. A saddle field ion argon sputter source was mounted to the outermost radiation shield (with the sputter gun also being kept at 77 K), making in-situ sputter cleaning of the gold crystal possible. This crystal cleaning method was employed in the later part of this project (see also Section 2.2).
5. The crystal mount was made high-temperature/UHV-compatible, thereby allowing for the rapid desorption of SAMs at 650 K several times during a single experiment and making it possible to anneal the gold surface at 750 K after sputter cleaning in situ.
6. The preamplifier for the bolometer signal was mounted on the neck of the helium cryostat, so that it can rotate with the bolometer as a diffraction scan is taken and the wires from the detector were glued to the helium cryostat, eliminating noise produced by wire movements.
7. The rotating wheel chopping the incident He beam was made infra-red-transparent so that the IR radiation reaching the bolometer through the collimator is no longer modulated and does not contribute to the a.c. signal amplified by the lock-in. This eliminates signal contributions that could interfere with diffraction peaks located near the specular signal due to the reflection of IR radiation off the crystal surface [26].

2.2. Substrate preparation

During the course of this study, two routes of substrate preparation have been followed. Before installation of the Ar sputter gun in the helium scattering chamber, clean gold surfaces were prepared in a separate UHV chamber. A Au(111) single crystal was cleaned by repeated cycles of Ar^+ sputtering and annealing to $\sim$750 K. Once the surface was confirmed to be clean and well-ordered by observing the well-known $23 \times \sqrt{3}$ surface reconstruction peaks using LEED or by an adequate specular reflection of a helium beam, the crystal was first covered with a protective layer of C10 by backfilling the chamber to a pressure of at least 5×10^{-5} Torr of C10 for at least 30 min, and then removed from that UHV chamber. After installing the crystal into the helium atom diffraction chamber, the gold surface was cleaned by desorbing the monolayer, i.e. heating the crystal to 650 K. During and subsequent to the desorption of the monolayer, the crystal was maintained within two concentric liquid-nitrogen-cooled enclosures. The cleanliness and order of the gold

surface was confirmed by helium atom diffraction. Surfaces were judged clean when:

1. the intensity of the specular reflection at 40 K was at least 15% of that of the incident beam, and the average value of the reflection coefficient was about 20%;
2. a well-resolved first order Au(111) diffraction peak was observed; and
3. the $23\times\sqrt{3}$ Au surface reconstruction peaks (1st, 2nd, and 3rd order) were observed.

As confirmed by these criteria, the crystal has routinely been kept clean in our apparatus for a week between experiments, provided that the crystal enclosures are maintained at liquid nitrogen temperature.

In the second route to substrate preparation, followed after the installation of the Ar sputter gun, clean Au(111) surfaces were also obtained by means of sputter and annealing cycles, but within the 77 K enclosures of the LEAD chamber. Again, the surface cleanliness was established with respect to the above three criteria.

Growths performed on crystals of varying degrees of cleanliness (specularity varying from 10% to 25%) resulted in consistent growth processes and growth times of the $c(4\times2)$ phase that were consistent with observed GIXD results [15,24].

2.3. Procedures for in-vacuo monolayer growth

2.3.1. Chemicals

Decanethiol (purity: 96–99%) was obtained from the Aldrich Chemical Company. Pumping on the sample at room temperature, until the vapor pressure stabilized, was used to remove the more volatile impurities (as confirmed by GCMS for similar chemicals after similar procedures.) Impurities with lower vapor pressures contribute little to the molecular flux at the crystal.

2.3.2. Molecular flux control and calibration

Growth experiments were carried out by exposing the crystal to a molecular flux produced by a nozzle at the end of the dosing line, which was fed by the vapor of decanethiol kept in an exterior reservoir. By regulating the thiol temperature from -10 to 50°C, the flux at the crystal face could be varied from less than 10^{14} molecules $cm^{-2}\,s^{-1}$ [less than 1 Langmuir (L) s^{-1}; for the conversion of flux to exposure; see Section 2.3.3] to over 10^{16}molecules $cm^{-2}\,s^{-1}$ (more than 100 L s^{-1}). The exposure was controlled through a combination of flux and exposure time, the latter being controlled by opening the shutter for a predetermined amount of time. As the shutter assembly was kept at 77 K along with the entire inner radiation shield, thiols that did not adhere to the crystal surface were rapidly removed, allowing exposure times to be controlled to 0.2 s. Dosing fluxes were calibrated by the two following methods, the results of which agreed within a factor of 2:

Method 1: The specular reflection was monitored during the deposition of a partial layer of decanethiol on a clean gold crystal kept at 40 K, where the sticking coefficient could be assumed to be unity. As the isolated organic molecules scattered the impinging He atoms in random directions, the resulting loss of specularity could be correlated to the accumulation of thiol molecules on the surface. This required an estimate of the scattering cross-section, which we obtain as follows. According to Comsa and Poelsema's work with CO on Pt(111) [27], the radius of the molecule's apparent cross-section (for a 6.0 meV helium beam) is 7.5 Å, about 6 Å more than the hard sphere radius of CO. This is larger than for He scattered by CO in the gas phase, which is believed to be due to the image charge in the conductive metal surface essentially doubling the molecule's polarizability, thus increasing the effective attractive dispersive forces. We roughly estimate the effective cross-section, Σ, of each C10 molecule in the initial stage of the growth by adding this 6 Å 'shadow' around the approximate 5×17 Å rectangle formed by the C10 molecule lying prone on the gold surface, and obtain a value of about 460 $Å^2$ (for 6.0 meV He atoms). A random accumulation of molecules with a density, n, and an effective area, Σ, on a clean gold surface will cause the specular intensity, I, to drop as $I=I_o e^{-n\Sigma}$, where I_o is the specular intensity of a clean gold surface. Writing the time (t) evolution as $n(t)=ft$ (with unity sticking

coefficient), we can determine the flux, f, from the $1/e$ decay time, τ, i.e. $f=(\Sigma\tau)^{-1}$. With the C10 reservoir at 0°C, we found $\tau=0.176$ s. This gives a flux of 1.24×10^{14} molecules $cm^{-2}\,s^{-1}$ or 0.8 L s^{-1}. The flux is found to scale linearly with vapor pressure, providing, for instance, a flux of 8.6 L s^{-1} when the thiol reservoir is kept at 23°C. Method 2: The flux was calculated using the geometry of the dosing system and vapor pressures of C10. According to kinetic gas theory, the flux of molecules (in molecules s^{-1}) through an orifice is [28]:

$$I=3.534\times10^{22}(PA)(MT)^{-1/2}\ s^{-1}, \quad (1)$$

where P is pressure in Torr, A is the area of the orifice in cm^2, M is the molecular mass in a.m.u. and T is the temperature in Kelvin. For C10 at 23°C (30 mTorr vapor pressure), this yields a flux of 1.3×10^{16} molecules s^{-1}. Taking into account the geometry of the nozzle (the ratio of length to radius is about 4) the flux on the surface of the crystal, 11 mm away, is estimated to be 3×10^{15} molecules $cm^{-2}\,s^{-1}$, or 20 L s^{-1} [28]. The thiol pressure at the dosing aperture was checked as follows. With all cryogenic surfaces at room temperature, vapors were run through the dosing line into the chamber, and the pressure rise was measured in the vacuum chamber. The product of the change in chamber pressure and the pumping speed of the diffusion pump yields the flux out, which is equal to the total flux from the dosing nozzle. The pressure rise in the scattering chamber was consistent with the sample vapor pressure as measured by a baratron. The growth rates determined on the basis of the above calibration were found to agree reasonably well (see below) with those measured by XPS [24,29] and X-ray diffraction [24]. Although the absolute value of the flux is only known with a 50% accuracy, the consistency of the flux determination among different LEAD runs and its stability during a run is better than 10%.

2.3.3. Conversion of flux to exposure

With the c(4×2) unit cell containing four molecules, its molecular density is 4.64×10^{14} molecules cm^{-2}, whereas that of the striped phase is 1.26×10^{14} molecules cm^{-2}, 27% that of the former. 1 L s^{-1} (the exposure rate produced by 10^{-6} Torr) of C10 at 300 K corresponds to a molecular impingement rate of 1.55×10^{14} $cm^{-2}\,s^{-1}$ [28] or only slightly more than one striped monolayer s^{-1}. Note that for all experiments, the nozzle of the dose line was always at 300 K (irrespective of the temperature of the thiol reservoir), and so the conversion factor (flux to exposure in Langmuir) was a constant (the only exception was one experiment with the reservoir and the nozzle at 330 K, which changed the conversion factor negligibly, as the flux depends on T only as one over the square-root).

2.3.4. Interrupted growth

At elevated temperatures, thermal motion causes a decrease in diffraction intensities (Debye–Waller effect), which makes helium diffraction difficult to observe at room temperature for C10 and many other SAM systems. Therefore, a methodology of interrupted growth was used to measure SAM growth rates. First the flux was calibrated by measuring the decay of the specular intensity while depositing a monolayer of molecules at 130 K. This layer was then brought to the designated growth temperature, the crystal temperature was lowered to 40 K and a LEAD scan was taken. Subsequent doses at the same flux were applied after the crystal was returned to the designated growth temperature. The time necessary to cool the crystal to 40 K is 20 min, and that needed to bring it back to about room temperature is 4 min.

In order to understand the initial growth process of the striped phase on the bare gold surface, other measurements were carried out. A bare crystal of gold at a variety of crystal temperatures (from 268 to 300 K) was exposed to a monolayer or a partial monolayer of decanethiol. These measurements verified a sticking coefficient of unity at all temperatures tested, for the decanethiol molecules on the bare gold surface.

2.4. Diffraction geometry

All diffraction measurements are done using an in-plane scattering configuration, i.e. the primary helium beam, the surface normal, and the detector

are all in the same plane. Diffraction patterns are taken by measuring the intensity of the scattered beam as a function of the polar angle as the detector is rotated in the scattering plane (for details see, Ref. [5] or [14]. The data in q-space can be transformed into momentum space by the use of the equation

$$\Delta k_{\parallel} = k_i(\sin\theta_f - \sin\theta_i) \quad (2)$$

where $\Delta k_{\parallel}$ is the momentum transferred parallel to the surface, q_f is the detector angle, and k_i and q_i are the incident wave number and angle, respectively. Diffraction patterns were taken mostly along the nearest-neighbor direction of the gold substrate (hereafter referred to as the $\langle 1\bar{1}0\rangle$ direction). This is where the main peak of the c(4×2) phase at $\Delta k_{\parallel} = -1.45$ Å^{-1} [indicating the hexagonal, $(\sqrt{3}\times\sqrt{3})$R30 thiol unit mesh] and the clearest pattern of the striped phase (diffraction peaks corresponding to the long axis of the molecules) can be found.

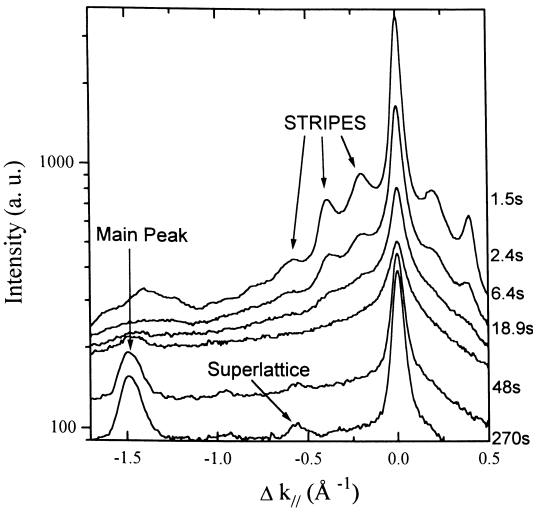

Fig. 2. Evolution of the LEAD pattern for various exposure times of a flux of 17.4 L s^{-1} of C10 at a crystal temperature of 5°C. The striped phase (characterized by diffraction peaks at multiples of $\Delta k_{\parallel} = 0.198$ Å^{-1}) forms immediately at low exposures. At intermediate exposures, we observe no clear diffraction features, indicating the lack of long-range order. Upon higher exposures, the c(4×2) phase with its most prominent main peak at $\Delta k_{\parallel} = -1.45$ Å^{-1} evolves, and later, the superlattice peak at $\Delta k_{\parallel} = -0.55$ Å^{-1}. The measurement procedure is one of interrupted growth, described in Section 2.3.4.

3. Results and discussion

3.1. Structural evolution

Before we quantify the growth, we will first give an overview of the structural evolution. Fig. 2 depicts several diffraction patterns from a crystal obtained after increasing amounts of exposure, showing the evolution of the monolayer from the striped phase to the dense c(4×2) phase. All scans have been taken along the $\langle 1\bar{1}0\rangle$ direction. The striped phase is identified by diffraction peaks at integer multiples of $\Delta k_{\parallel} = 0.198$ Å^{-1} [4], and the c(4×2) structure is identified by a large diffraction peak at $\Delta k_{\parallel} = -1.45$ Å^{-1} (referred to here as the 'main' peak) and smaller superlattice peaks, for instance at $\Delta k_{\parallel} = -0.55$ Å^{-1} [7]. The intermediate scans show no diffraction and, thus, no long range order, and we refer to this region as the intermediate phase [24].

In Fig. 3, we plot the evolution of the different features as a function of exposure. The intensity (throughout the paper 'intensity' is to be understood as 'integrated intensity') of the second-order

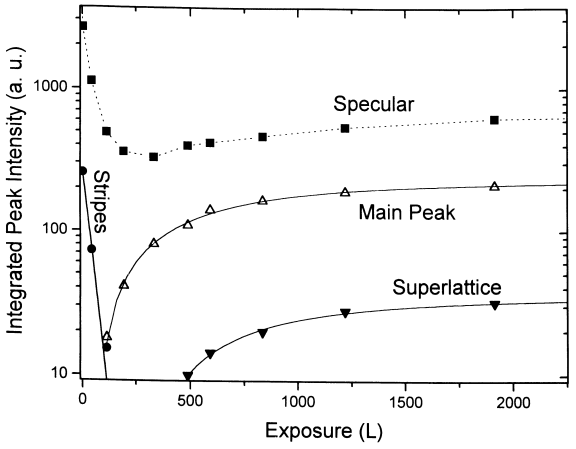

Fig. 3. Evolution of integrated peak intensities deduced from the LEAD signals as a function of exposure under the conditions given in Fig. 2. C(4×2) main peak and superlattice intensities are fitted to a Langmuir growth curve: $I = A[1 - e^{-(t-t_0)/\tau}]$ (Eq. 3). The stripes intensities are fitted to an exponential decay: $e^{-t/\tau}$ yielding decay times (Table 1). The specular data are simply connected by a line to guide the eye.

striped-phase diffraction peak at $\Delta k_{\parallel} = -0.396\,\text{Å}^{-1}$ (Fig. 2) is used as a measure of striped phase evolution, and the intensity of the c(4×2) main peak at $\Delta k_{\parallel} = -1.45\,\text{Å}^{-1}$ (Fig. 2) and superlattice peak are used to monitor the c(4×2) evolution. The intensity of the specular peak is, in turn, determined by the atomic flatness of the surface, by the amplitude of the potential corrugation and by the amount of inelasticity experienced by the He atom [27].

One can see that the striped phase (shown as filled circles in Fig. 3) grows immediately on the bare gold surface. Indeed, a full striped monolayer was reproducibly achieved with an exposure of about 1 L of decanethiol. The intensity of the striped pattern decreases and disappears with further exposure (typically on the scale of about 100 L), correlated with a decrease in the specular intensity (filled squares in Fig. 3), indicating a greater degree of disorder in the intermediate phase. We infer that this greater disorder is caused by additional molecules adsorbing non-uniformly on or within the striped phase regions, yet still at coverages that are lower than those needed to nucleate the c(4×2) phase. Upon further exposure, the c(4×2) phase (in Fig. 3, open and filled triangles for the main and superlattice peak, respectively) grows out of the intermediate phase establishing again the long-range order of the film and therefore producing a recovery of the specular intensity. The c(4×2) phase saturates after exposures that, for the conditions of Fig. 3, are approximately 2000 L.

A Langmuir growth model fits well with both the main and c(4×2) superlattice intensity evolution:

$$I = A[1 - e^{-(t-t_o)/\tau}] \quad (3)$$

where t_o is the time before the onset of the growth of the main peak. The characteristic growth times, $\tau_{(\text{main})}$ and $\tau_{(\text{superlattice})}$, and the thiol 'acceptance coefficients' as determined by the growth of the main peak, obtained under several different growth conditions, are shown in Table 1. The average 'acceptance coefficient' is the molecular uptake rate divided by the flux to the crystal surface:

$$\frac{(\Theta_{\text{hex}} - \Theta_{\text{nuc}})/\tau_{(\text{main})}}{\text{flux}},$$

where (Θ_{hex}) is the density of the hexagonal phase [nominally the same as the density of the c(4×2) phase; see Section 2.3.3)], and Θ_{nuc} is the density of the intermediate phase at the onset of nucleation of the hexagonal phase (see Section 3.3.1). Unlike the term 'sticking coefficient', 'acceptance coefficient' refers to the probability of a molecule to be chemisorbed into the forming SAM. The two terms may be thought of as the same for the initial growth of the striped phase on bare gold.

As stated before, the striped phase is found to grow with an acceptance (sticking) coefficient close to unity. The subsequent decrease in the intensity of the striped phase diffraction peaks can be used to estimate the subsequent thiol uptake. The intensity of the striped phase peak can be fitted to an exponential decay function, $e^{-t/\tau}$, yielding the decay time, t_d. This decay time represents the rate of modification of the striped surface by thiol molecules adsorbing on to it. Again, the flux of adsorbing molecules equals $(t_d S)^{-1}$, where S is the cross-section of a molecule to a helium beam [27]. A complication here is that the cross-section of a newly incorporated molecule is not known, as the perturbation that it introduces may extend to its neighbors to some degree. If we assume a cross-section of $4.2\times10^{-14}\,\text{cm}^2$ (which is probably known within a factor of 3), we can calculate the acceptance coefficient for the decay of the striped phase. Because of the uncertainty of the value of S, this acceptance coefficient is affected by the same error.

Two recent studies have reported that the striped phase grows from vapor deposition on the bare gold surface with approximately the same acceptance coefficient as subsequent growth, implying a single step, simple Langmuir growth process [16,22]. This acceptance coefficient is on the order of 10^{-3}. The above data (Figs. 2 and 3 and Table 1) clearly show that the growth of C10 from vapor *cannot* be described with *a single* time constant. In fact, the typical time scales for the formation of the stripes and that for the c(4×2) differ by a factor of about 500 (for the conditions of Fig. 3; see also Table 1). Our discovery of this two step growth process has been subsequently confirmed by recent studies with XPS [24,29] and GIXD [21,24]. In agreement with these experi-

Table 1
Growth parameters of decanethiol SAM on Au(111). '$\tau_{(\text{main), measured}}$' and '$\tau_{(\text{superlattice), measured}}$' are the growth times measured from fitting the area of the $\Delta k_{\parallel} = -1.45$ Å^{-1} c(4×2) main peak, and $\Delta k_{\parallel} = -0.55$ Å^{-1} superlattice peak, respectively, to the Langmuir growth model. '$\tau_{(\text{main), calculated}}$' is the c(4×2) main peak growth time as predicted by Eberhardt's growth model [15]. '$\tau_{(\text{stripes decay})}$' is the time measured from fitting the area of the $\Delta k_{\parallel} = \pm 0.198$ Å^{-1} stripes peak to an exponential decay model. Acceptance coefficients are defined as the molecular uptake rate divided by the flux. The large error in the 300 K main peak growth times are due to the fact that hexagonal peaks were not grown to completion because of the excessive amount of time required, which often resulted in nozzle clogging. Fluxes are accurate to within a factor of 2 of the absolute value given. However, between experiments, the relative error is less than 10%

Crystal temperature	300 K		278 K		268 K	
Flux (L/s) (10% relative error)	1.6	17.4	4.7	17.4	4.7	17.4
$\tau_{(\text{main), measured}}$ (s)	12 000 ± 4000	***	359 ± 27	33.4 ± 1.6	60.5 ± 5.6	33.5 ± 6.5
$\tau_{(\text{main), calculated}}$ (s)	10 000 ± 1000	***	270 ± 30	22.0 ± 2.5	10.2 ± 1.2	1.34 ± 0.09
$\tau_{(\text{stripes decay})}$ (s)	80 ± 15	7.77 ± 0.92	28.9 ± 3.2	1.85 ± 0.18	16.4 ± 1.5	2.84 ± 0.09
$\tau_{(\text{superlattice), measured}}$ (s)	***	***	341 ± 98	33.4 ± 3.0	51.3 ± 32	***
Main acceptance coefficient (×10^5)	8.4 ± 3.5	***	95 ± 9	280 ± 20	560 ± 50	270 ± 50
Stripes acceptance coefficient (×10^4)	13 ± 2	12 ± 1.4	12 ± 1.4	47 ± 5	21 ± 2	32 ± 2
Ratio of acceptance coefficient (main/stripes)	0.07	***	0.79	0.60	2.7	0.84

ments [21,24,29] only the final growth step – that of the c(4×2) standing up phase growing out of the nucleation density intermediate phase – appears to follow a first-order Langmuir model as demonstrated by the good fit of the growth curves to the Langmuir model. Possible reasons for the apparent conflict between diffraction and STM results [22] (in which, as indicated above, a single-step, Langmuir model is used to explain the data) are discussed in Ref. [25], and are the subject of current investigations in our laboratory.

As the growth of the stripes is distinctly different in nature and speed from the subsequent growth of the SAM monolayer, it is worthwhile to investigate whether more subtle distinctions exist between the evolution of the intermediate phase and the final growing of the c(4×2) phase that follows it. First-order Langmuir growth states that $d\Theta/dt \propto (1-\Theta)$, where Θ is the coverage. This presumes that (1) if a molecule strikes a site that is not occupied, it stands a *coverage-independent* probability of chemisorbing, and (2) if a molecule strikes a site that is occupied, it must desorb. This is true only if the stay time of the admolecule on the occupied site is much less than that required for the admolecule to migrate to a free site. These criteria are only met in the final stage of SAM growth when a nucleation density intermediate phase grows into islands of the standing-up phase. Until then, the growing monolayer consists of a single phase (in equilibrium growth) or a variety of different phases (in non equilibrium growth) that change character as the layer matures. The stripes, intermediate phase, and c(4×2) have different structures and offer a different stay time to an additional molecule arriving at the surface and different accessibility to the gold substrate.

The stripes acceptance coefficient (which is calculated from the speed in which the stripes turn into the intermediate phase, Table 1) and the acceptance coefficient for the main c(4×2) peak (which is connected with the intermediate phase turning into the standing up phase) cannot be compared with absolute precision because of the uncertainty in the apparent size of an admolecule's perturbation to the striped surface as mentioned above. However, we can see that (and explain why) the behavior of the two acceptance coefficients seems to respond differently to temperature changes. While both the main peak and stripes acceptance coefficients increase with a decrease in crystal temperature from 300 to 268 K, the main peak acceptance coefficient increases by well over an order of magnitude *more* than that of the stripes (see Table 1). This can be explained when one considers two competing factors that are affected by crystal temperature: (1) increased crystal temperature results in a loss in admolecule stay time

and will tend to lower acceptance coefficients; and (2) the increased thermal disorder to the stripes layer with increased temperature increases the probability for admolecules to make contact with the gold surface, increasing the acceptance coefficient, and therefore tends to counteract the effect of the loss in staytime. However, the intermediate phase is shown by X-ray scattering [24] and STM [22] to be largely disordered at room temperature and by LEAD (in this work) to be disordered even at 40 K. Therefore, increasing the crystal temperature increases access to the gold surface more in the case of the more ordered striped phase. With much less of the second of the above two *competing* temperature effects, the rate of growth of the $c(4\times2)$ phase should have a stronger temperature dependence, as is found experimentally.

For the sake of completeness, we also note that in some cases it appeared impossible to grow a $c(4\times2)$ phase even after extremely long exposures. The result was typically an intermediate coverage structure (Fig. 4) showing a striped like pattern with a periodicity of 28.7 Å, or 11% shorter than that of 'normal' C10 stripes. The appearance of these 'kinetic traps', or local minima in the free energy function, relates to results reported by others [12], where vapor phase deposition was also used. The fact that it was never observed using GIXD [21,24,29] might be connected to the interrupted growth mode used in the present work (see Section 2.3). According to our experience, the growth is more likely to become kinetically trapped at slow rates (i.e. high T and low P) and in the presence of longer waiting periods at intermediate stages. An effective technique for consistently growing the full density, $c(4\times2)$, phase involved dosing a crystal (10–20 L s^{-1}) while ramping the crystal temperature from 240 to 300 K at about 10 K min^{-1} [25]. The success of this technique implies that the nucleation of the $c(4\times2)$ phase is assisted by disorder and/or by an inhomogeneous coverage with a large number of nucleation centers. Although the study of kinetic traps is of substantial interest, we did not pursue it systematically. Because of the importance of the nature, concentration and distribution of defects in understanding kinetic traps, one would need in this case, a combined diffraction/STM approach.

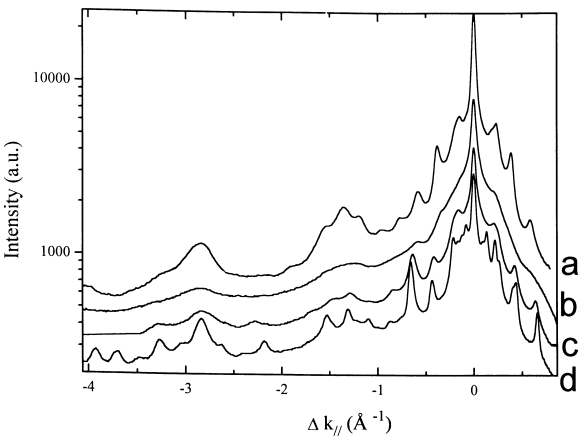

Fig. 4. Evolution of the LEAD pattern ending in a kinetic trap formed at a crystal temperature of 300 K and flux of 17.4 L s^{-1}: (a) after 110 L exposure, the striped phase (characterized by diffraction peaks at multiples of $\Delta k_{\parallel}=0.196$ Å^{-1}) is obtained; (b) after 1000 L exposure; (c) after 10 000 L exposure, a 10% smaller periodicity striped pattern arises (characterized by diffraction peaks at multiples of $\Delta k_{\parallel}=0.215$ Å^{-1}); (d) after 340 K anneal, peaks narrow (domain size increases) and $\Delta k_{\parallel}$ increases by 3% to 0.219 Å^{-1} (average unit mesh shrinks further by 3%).

3.2. Flux and temperature dependence of the growth rate

A natural step towards a better understanding of the processes involved in the growth is the investigation of their dependence on the incoming flux, P, and substrate temperature, T. As mentioned in the introduction, a GIXD study recently found [15] that, under certain conditions (high flux and low temperature), the growth rate of the $c(4\times2)$ increases no longer linearly but *quadratically* with P. This rate, R (in s^{-1}), is described by Eberhardt et al. [15] as:

$$R=A_1Pe^{E_1/T}+A_2P^2e^{E_2/T} \quad (4)$$

with

$A_1=7.4\times10^{-10}$;

$A_2=2.7\times10^{-43}$ s;

$E_1=0.30\pm0.05$ eV (corresponding to 3.48×10^3 K);

$E_2=2.15\pm0.22$ eV (corresponding to 2.5×10^4 K);

$P=$ the impingement rate (L s^{-1}); and

T = the crystal temperature (K).

In what follows, we will test the consistency of this model with our LEAD data (see also Table 1) – confirming the above growth rates in the linear regime and the existence of the quadratic regime in the pressure dependence of the growth rate, R. Furthermore, we will also show that at lower temperatures, this trend is inverted in the sense that R becomes weakly dependent on P.

According to Eq. 4, at 300 K and an impingement rate of 1.6 L s^{-1} (Table 1), the growth rate, R, is well within the linear regime. Our data agree quantitatively with the GIXD data [15,24].

Furthermore, the rate of growth is linear with pressure. Because of the very slow growth rate at room temperature, the linearity of the growth rate with flux has to be deduced from a comparison of the decay times of the striped phase under the two different flux conditions. When the flux is increased by a factor of ten, the characteristic decay time decreases by the same factor. In other words, the corresponding acceptance coefficients are equal within error. A decrease in T leads to an increase in the growth rate. For the two impingement rates used in this study, a temperature decrease to 278 K puts R in the quadratic regime. Although the 278 K growth rates derived from our LEAD data do not agree exactly with those predicted by Eq. 4, they clearly support the presence of a quadratic dependence of R on P. This can be seen from the fact that when the flux is increased by a factor of 3.7, the c(4 × 2) acceptance coefficient is also tripled, and the characteristic growth time, $\tau_{(\mathrm{main})}$, decreases by a factor of 10.7, which is close enough to $(3.7)^2 = 13.7$. Within error bars, the decay time of the striped phase also decreases by the same factor at this temperature. A growth rate quadratically dependent on pressure may be explained by the possible existence of a bimolecular process such as dimerization of the thiols [8] or the formation of H_2 through cleavage of the S–H bond. The quadratic dependence could also be the result of incident molecules interacting with the population of physisorbed admolecules, either increasing the physisorbsion probability of incident molecules, or increasing the stay time of physisorbed molecules.

It is very instructive to test the limits of the above scenario by further decreasing T. Whereas one might expect simply a further increase of R governed by the P^2 contribution, the measured growth rates for 268 K not only deviate strongly from the prediction of Eq. 4, but the trend is inverted, and an increase in P causes a decrease in the c(4 × 2) acceptance coefficient, which means that the growth rate *increases less than linearly* with the flux. Fig. 5 aims at presenting a pictorial view of the situation showing the pressure dependence (P^0, P^1 or PP^2) of the growth rate of the c(4 × 2) phase in a plane where the coordinates are the crystal temperature and the thiol flux. Data points simply represent conditions under which the growth of the c(4 × 2) phase has been monitored by LEAD. The boundaries between regions are not sharp, but should be thought of as transition regions. The P^1–P^2 transition has been well documented by GIXD [15] and confirmed by the present work. The P^2–P^0 transition is placed between the two growth observations (at 268 K) that defined the transition to a region where the dependence of the growth rate on the decanethiol vapor pressure is less than linear. The slope of the line has been drawn, assuming Arrhenius behavior, to present a family of conditions under which a full overlayer of thiols would exist *over* the growing intermediate phase (see below).

If the growth of a SAM is accomplished through the assimilation of admolecules that are physisorbed on its surface, increasing the flux to the surface increases the population of physisorbed molecules, which increases the growth rate. However, once a full coverage of physisorbed molecules on the surface of the forming SAM is attained, a further increase in flux cannot increase the monolayer growth rates.

3.3. Annealing and growth

3.3.1. Annealing and phase coexistence

When P and T are varied over a large range so that the growth behavior changes qualitatively, as seen in Section 3.2), it is particularly important to investigate whether a SAM grown under certain conditions reflects an equilibrium or a kinetically limited (non-equilibrium) structure. Annealing is a way to address this issue, and here we discuss a

few effects related to the annealing at different stages of the growth.

X-ray measurements [24] have shown that, under equilibrium growth conditions, the phase boundaries between the three phases in coverage space are $\Theta \sim 0.27$ (stripes – intermediate phase) and $\Theta \sim 0.47$ [intermediate – c(4×2) phase]. Furthermore, using GIXD [24], a distinction can be made between high-temperature and low-temperature growth conditions. In the first case, from the beginning of the growth, the islands coalesce with each other, and the domain size observed by X-rays is limited only by the size of the gold terraces. In the low-temperature case instead (below 285 K), the domain (island) size observed by X-rays is smaller, and grows monotonically with the coverage of the c(4×2) phase.

A typical non-equilibrium effect is the shifting of phase boundaries, e.g. the appearance of a certain phase at an excessively high or low coverage. Indeed, in several experiments at a lower temperature, we observed a premature onset of the c(4×2) phase. Fig. 6 shows a layer grown to intermediate coverage at 268 K with a clear diffraction peak at $\Delta k_{\parallel} = -1.45$ Å^{-1} representing the standing-up phase [10] coexisting with some stripes islands indicated by small stripes peaks. After heating the layer to 300 K for 4 min (again, all LEAD scans were taken at 40 K), the intensity of the main c(4×2) peak *decreased*, which, at 300 K, cannot be explained by desorption effects. In this case, the layer was only annealed closer to its equilibrium state (with molecules in the intermediate phase not contributing to diffraction peaks), indicating that the onset of the standing up phase had been premature. It is interesting to note that the decrease in specular indicates that in this case, annealing to a lower energy state produces a more "bumpy" surface. This is understandable when we recognize that the intermediate phase is less ordered than either the stripes or the c(4×2). We believe that the mechanism for this premature onset of the standing up phase is related to the fact that the density of molecules *locally* but *not globally* exceeded the threshold value for the stand-

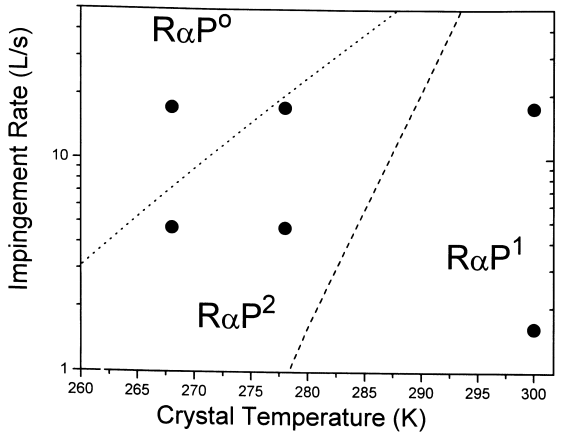

Fig. 5. Summary of the growth rate dependence on thiol pressure (i.e. flux to the crystal surface). For a high T and low P, the c(4×2) phase growth rate increases linearly with pressure, whereas for a lower T and higher P, the growth rate increases *quadratically* with pressure. Still lower T and higher P lead to growth rates that are almost independent of pressure. The lines separating these regimes (not to be confused with fits to the data points) are not to be seen as sharp boundaries but as indications of transition regions. The P^1–P^2 transition was well defined by GIXD growth data [15] and verified in the present work. The data points plotted represent conditions under which SAM growth data were collected.

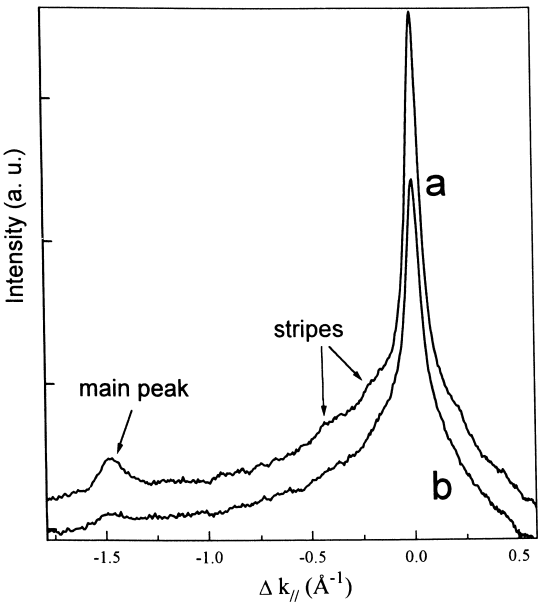

Fig. 6. Example for non-equilibrium growth effects, where premature growth of the c(4×2) phase is obtained. (a) Pattern produced by a layer deposited at 4.7 L s^{-1} for 120 s on a 278 K crystal and cooled to 40 K. (b) The same layer after a 270 s anneal at 300 K.

ing up phase. This is a typical non-equilibrium growth effect, where, due to limited mobility on the surface, the flux of incoming molecules cannot be appropriately accommodated.

3.4. Adsorption energetics and admolecule residence times

In order to shed more light on the molecular-level processes involved in the fairly complex growth scenario outlined in the previous sections, we set out to measure the energetics and characteristic time scales of the adsorption of molecules that may occur on top of layers with different coverages. For this, we employed the methods of specular intensity recovery observation (SIR) and also a kind of temperature-programmed desorption (TPD) measurement in which the surface coverage was monitored by observing the changes induced in the He atom reflectivity.

3.4.1. Specular recovery

The high sensitivity of helium scattering to changes on the surface was utilized to investigate the dynamic processes related to the growth. During and after dosing of the thiols, the specularly reflected helium beam was recorded in real time. Typically, the signal dropped significantly during the dose. After closing the thiol shutter, the specular signal recovered and asymptotically leveled off to a new equilibrium value corresponding to the respective coverage. The half-time for the specular recovery is characteristic for a given coverage and temperature and contains information about processes like (partial) desorption (e.g. admolecules desorbing from the organic surface) or reordering/lateral diffusion of molecules that did or will eventually chemisorb. Fig. 7 shows a typical SIR scan carried out at 258 K. We determine the time constant, τ_{SR}, of the recovery by fitting to an exponential

$$I(t)=I_o[1-e^{-(t-t_o)/\tau_{SR}}] \quad (5)$$

Our attempts at determining which part of the recovery is due to desorption and which part is due to reordering are described here below. Doses of less than a single Langmuir of exposure ('small doses') on striped or intermediate phase SAMs result in negligible thiol uptake due to the small acceptance coefficient (see Table 1). Therefore, the specular recovery after a small dose is governed by desorption of admolecules, and the specular recovers to its initial value. Higher doses (hundreds of Langmuirs) result in a substantial population of additional molecules incorporated into the incomplete SAM indicated by a specular recovery that does not reach its initial value.

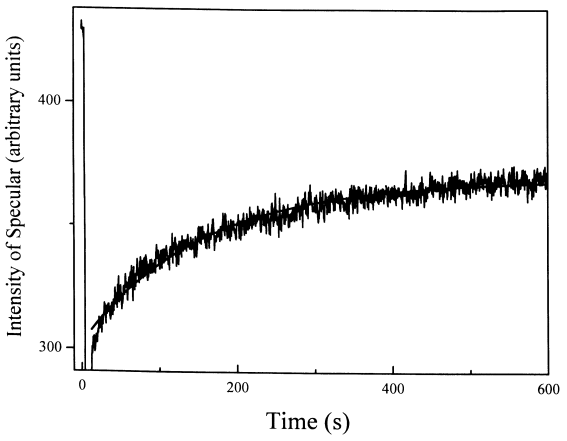

Fig. 7. Recovery of the specularly reflected He atom beam after dosing 10 L of C10 on a striped phase monolayer at 258 K. The rapid initial drop (at $t=0$) is related to an electronic perturbation at the beginning of the dose. From the time constant of the recovery after the end of the dose, we can obtain information on the adlayer energetics.

The results of a 0.2 L dose and a 300 L dose on a striped phase surface at 300 K are shown in Fig. 8. The acceptance coefficient is about 10^{-3} (see Table 1), so only the larger dose results in a substantial amount of thiol uptake (about 34% of a striped monolayer). The small dose results in a quick recovery (limited by the 1 s integration time of the lock-in amplifier), indicating the short residence time of the incident molecules on the surface under these conditions. The ordering time recorded after the 300 L dose (after a quick initial rise) was greater than 200 s, indicating a much longer time required for the freshly augmented layer to order.

Further analysis of the specular recovery after a small dose indicates that desorption of newly deposited molecules on the striped layer is not first-order Langmuir desorption, because the spec-

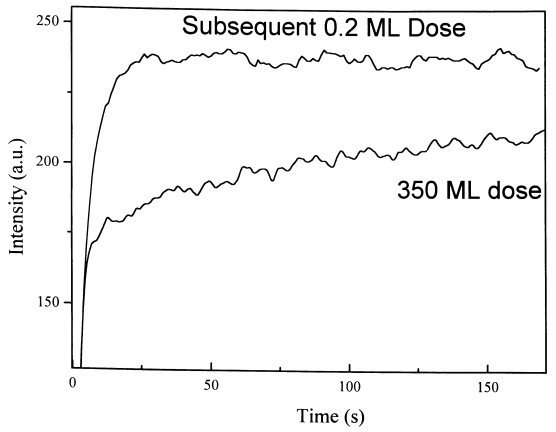

Fig. 8. Decoupling desorption and ordering. The top specular recovery curve on a 300 K striped surface indicates the near immediate ($\tau < 2$ s) desorption of a 0.2 L dose after a 0.1 s exposure. After, a 300 L exposure on the same surface, considerable adsorption of admolecules results in an additional, longer ($\tau > 200$ s) recovery.

ular recovery cannot be fitted by a single exponential, but seems to require several time constants [25]. Langmuir kinetics assumes that all adsorption sites are equivalent. Therefore, the population of these molecules, Θ, would decrease according to: $d\Theta/dt = -k\Theta$ (k is a constant), which would yield a specular recovery of a single exponential (Eq. 5). Our data [25] imply that not all adsorption sites are equivalent – molecules that find lower-energy configurations remain on the surface for a longer time, resulting in a longer recovery time. This is relevant to monolayer growth because a longer residence time results in a better chance of chemisorbing.

The temperature dependence of the recovery rates for small doses can be analyzed on the basis of an Arrhenius relation [rate $= \nu \exp(-E_a/kT)$]. However, due to the well-known problems related to a reliable determination of the pre-exponential factor, ν, and possible small differences in the state of the underlying layer at different temperatures [23,30], we consider our result for the activation energy, E_a, only as an estimate. Assuming, as customary, $\nu = 10^{13}\ s^{-1}$, we obtain $E_a = 0.74$ eV for admolecules on a stripes layer based on a 9 s recovery time at 268 K.

3.4.2. Temperature-programmed desorption

Specularity-detected TPD is another method to determine adsorption energies (or, more precisely, desorption enthalpies). The experiment is performed by ramping the crystal temperature with a heating rate, β while observing the desorption peak temperature, T_m, by monitoring the derivative of the specular reflection of the helium beam from the surface. TPD is employed to measure the adsorption energy of molecules on the surface of the c(4 × 2) phase because in this case, the specular recovery times were difficult to determine (as the specular changes were small). Layers were deposited at 40 K on top of a full c(4 × 2) layer. Before desorbing, these molecules ordered very well, providing excellent diffraction patterns. The ordering, observed as a specular rise while heating, started almost immediately at 40 K, but rose most rapidly between 90 and 140 K. As the crystal temperature reached 232 K, the overlayer desorbed, leaving the c(4 × 2) monolayer surface free. Note that because the adsorbed overlayers are so well ordered, the desorption of the admolecules corresponds to a *decrease* in the specular intensity [25]. The energy of desorption can be estimated by the Redhead equation [30]:

$$E_{des} = T_m\left[\ln\left(\frac{\nu T_m}{\beta}\right) - 3.46\right] \quad (6)$$

where, β is 0.04 K s^{-1}. This yields a desorption energy of 0.70 eV for $T_m = 232$ K. At 40 K, the surface of the *overlayer* is very regular, with a specular peak height approximately eight times that of the underlying c(4 × 2) surface, which, together with high diffraction intensities, implies that the molecular overlayer is capable of healing away some of the defects of the underlying c(4 × 2) surface. Further analysis of the structure of the overlayer is contained in the thesis of one of the authors (P.S.) [25].

3.4.3. Comparison of energies

Based on the measured energies (see Table 2), the following picture arises. The bulk interaction energy of C10 is 0.67 eV (as deduced from the heat of vaporization). For a C10 admolecule on top of a c(4 × 2) SAM, the adsorption energy is

Table 2
Summary of interaction energies for C10 (see Section 3.4 for discussion)

E (C10 bulk condensation)	0.67 eV	[31]
E (C10 on mature intermediate phase)	0.65 eV	Present work
E [C10 on c(4 × 2)]	0.70 eV	Present work
E (C10 on stripes)	Ranges between 0.74 and 0.80 eV	Present work
E [C10 on Au(111)], (physisorption)	1.10 + −0.05 eV	[23]
E [C10 on Au(111)], (chemisorption)	1.28 + −0.05 eV	[23]

0.70 eV. For C10 on a striped-phase SAM, we find a slightly higher value of between 0.74 and 0.80 eV (as discussed above, more than one time constant is required to fit the specular recovery curves, indicating the presence of sites of different energy), which is understandable, given that a molecule on top of a striped phase layer is closer to the gold substrate, so that the gold–overlayer interaction has to be taken into account. From the 0.2 s stay time of admolecules on a mature intermediate phase (see Section 2.2), we can estimate an adsorption energy of 0.65 eV on the mature intermediate phase. In this series of Van der Waals-dominated interactions, the strongest is, of course, found for C10 directly physisorbed on Au(111). Its high energy of 1.1 eV is close to its (sulfur–gold) chemisorption energy of 1.28 eV, as reported by Lavrich et al. [23]. In fact, for only slightly longer chains (C14), the physisorption and the chemisorption energy are equal [23]. This explains the near unity acceptance coefficient of C10 on the clean substrate.

We presume that the longer an admolecule resides on the surface, the greater the probability is for it to chemisorb directly to the surface or join another molecule to chemisorb in a possible bimolecular process. As the admolecule stay time has an exponential dependence on the surface temperature, the crystal temperature should govern the growth rate, R, and the locations of the boundary between the quadratic and linear growth regimes and the boundary between the quadratic and less-than-linear growth regimes. However, as the crystal temperature will also have other growth rate effects such as the rate at which physisorbed molecules overcome the activation barrier to chemisorption, the temperature dependence of the location of these boundaries is not that of a single exponential.

4. Summary and conclusion

Using LEAD, we have performed a detailed study of the kinetics and energetics of the growth of C10 on Au(111) by molecular beam deposition. Exploiting the unique surface specificity of atomic scattering, we followed the evolution of the various phases: from the striped phase to the intermediate phase to the c(4 × 2) phase. Clearly, this process is not adequately described by only one time constant. We identify two and possibly three steps with different acceptance coefficients and temperature dependencies. This complexity is ultimately a consequence of the numerous degrees of freedom of this archetypal self-assembling system with its multiple interactions. The observation that the initial growth of the striped phase proceeds much faster than the subsequent growth [the decay of this phase and growth of the c(4 × 2) phase thereafter] may be understood in terms of the fact that the subsequent growth occurs on a preexisting organic layer that evolves with exposure until it reaches the critical density required for nucleation of c(4 × 2) islands. The underlying striped or intermediate phase layer both limits the admolecule's access to the gold surface and shortens the residence time of the admolecule on the organic surface.

The P^2 effect, i.e. the increase of the c(4 × 2) growth rate with the *square* of the pressure at high P and low T, (another complexity of this system found recently by GIXD [14]) was confirmed,

showing that the GIXD result was not a consequence of X-ray exposure.

By investigating the effects of annealing at an intermediate stage, we could demonstrate important differences between equilibrium and non-equilibrium growth. At intermediate coverages, for extreme non-equilibrium growth conditions, the coexistence of different phases can be observed, but appropriate annealing procedures bring the film back into its equilibrium structure.

Another peculiarity of this system is the occurrence of kinetic traps that are more likely to occur under the conditions of slow growth (high T and low P). These kinetic traps are lower coverage phases that prevent the growth of a full coverage [c(4×2)] phase. Although it is clearly possible to grow the c(4×2) from vapor, these kinetic traps may have been the reason for problems that our and other groups have experienced in the past with vapor phase growth.

We also determined some of the energy parameters and molecular time scales involved in the growth. The physisorption energy of admolecules as a function of coverage [from C10 on bare gold to C10 on the striped phase to C10 on the c(4×2) phase] largely exhibits an understandable decrease with increasing distance from the substrate. Although it is very difficult to fully characterize the energetics of all the processes involved, we hope that our data help to further promote the understanding of this complex problem.

These results show that LEAD is a very sensitive tool that can help to monitor a multitude of processes occurring on the surface of SAMs. Clearly, the scenario obtained for the growth of C10 on Au(111) is much more complex than that seen in previous investigations, and not all details are fully explored and understood. However, we have at least been able to answer some open questions and pose a few others that, when answered, will likely lead to the full understanding of the kinetic behavior of this archetypal membrane-forming system.

Acknowledgements

We thank L. Darazio for his input in the surface machine renovations. We benefited greatly from interactions with D. Lavrich and P. Fenter. P.S. would like to acknowledge a useful discussion with M. Grunze and F.S. acknowledges support by the Deutsche Forschungsgemeinschaft. This work has been supported by the Materials Science Program of the Office of Basic Energy Sciences of DOE under grant DE-FG02-93ER45503 and in part, by the NSF under the Princeton MRSEC grant.

References

[1] A. Ulman, An Introduction to Ultrathin Organic Films: From Langmuir–Blodgett to Self-Assembly, Academic Press, Boston, MA, 1991.
[2] G.M. Whitesides, P.E. Laibinis, Langmuir 6 (1990) 87.
[3] L.H. Dubois, R.G. Nuzzo, Annu. Rev. Phys. Chem. 43 (1992) 437.
[4] N. Camillone III,, P. Eisenberger, T.Y.B. Leung, P. Schwartz, G. Scoles, G.E. Poirier, M.J. Tarlov, J. Chem. Phys. 101 (1994) 11031.
[5] N. Camillone III,, T.Y.B. Leung, P. Schwartz, P. Eisenberger, G. Scoles, Langmuir 12 (1996) 2737.
[6] G.E. Poirier, M.J. Tarlov, H.E. Rushmeier, Langmuir 10 (1994) 3383.
[7] N. Camillone III,, C.E.D. Chidsey, G.-Y. Liu, G. Scoles, J. Chem. Phys. 98 (1993) 3503.
[8] P. Fenter, A. Eberhardt, P. Eisenberger, Science 266 (1994) 1216.
[9] E. Delamarche, B. Michel, H.A. Biebuyck, C. Gerber, Adv. Mater. 8 (1996) 719.
[10] L. Strong, G.M. Whitesides, Langmuir 4 (1998) 546.
[11] R. Gerlach, G. Polanski, H.-G. Rubahn, Appl. Phys. A 65 (1997) 375.
[12] F. Balzer, R. Gerlach, G. Polanski, H.-G. Rubahn, Chem. Phys. Lett. 274 (1997) 145.
[13] L.H. Dubois, B.R. Zegarski, J. Chem. Phys. 98 (1993) 678.
[14] N. Camillone, Ph.D. thesis, Princeton University, 1994.
[15] A. Eberhardt, P. Fenter, P. Eisenberger, Surf. Sci. 397 (1998) L285.
[16] R.C. Thomas, L. Sun, R.M. Crooks, A.J. Ricco, Langmuir 7 (1991) 620.
[17] M. Buck, M. Grunze, J. Vac. Sci. Technol. A 10 (1992) 926.
[18] W. Pan, C.J. Durning, N.J. Turro, Langmuir 12 (1996) 4469.
[19] S. Xu, S. Cruchon-Dupeyrat, J.C. Garno, G.-Y. Liu, G.K. Jennings, T.-H. Yong, P.E. Laibinis, J. Chem. Phys. 108 (1998) 5002.
[20] K. Peterlinz, R. Georgiadis, Langmuir 12 (1996) 4731.
[21] A. Eberhardt, Ph.D. thesis, Princeton University, 1996.
[22] G.E. Poirier, E.D. Pylant, Science 272 (1996) 1145.
[23] D.J. Lavrich, S.M. Wetterer, S.L. Bernasek, G. Scoles, J. Phys. Chem. 102 (1998) 3456.
[24] F. Schreiber, A. Eberhardt, T.Y.B. Leung, P. Schwartz,

S.M. Wetterer, D.J. Lavrich, L. Berman, P. Fenter, P. Eisenberger, G. Scoles, Phys. Rev. B 57 (1998) 12476.
[25] P. Schwartz, Ph.D. thesis, Princeton University, 1998.
[26] N. Camillone III,, C.E.D. Chidsey, G.-Y. Liu, T.M. Putvinski, G. Scoles, J. Chem. Phys. 94 (1991) 8493.
[27] G. Scoles (Ed.), Atomic and Molecular Beam Methods Vol. II Oxford University Press, Oxford, 1992..
[28] G. Scoles (Ed.), Atomic and Molecular Beam Methods Vol. I Oxford University Press, Oxford, 1992..
[29] P. Fenter, F. Schreiber, L. Berman, G. Scoles, P. Eisenberger, M.J. Bedzyk, Surf. Sci. 412 (1998) 213.
[30] D.A. King, Surf. Sci. 47 (1975) 384.
[31] D.R. Lide (Ed.), Handbook of Chemistry and Physics 73rd ed., CRC Press, London, 1992..